Higher-twist contributions, quantum chromodynamics, and inclusive meson photoproduction at high p_T

J. A. Bagger
Department of Physics, Princeton University, Princeton, New Jersey 08544

J. F. Gunion
Department of Physics, University of California at Davis, Davis, California 95616
(Received 26 May 1981; revised manuscript received 15 January 1982)

We investigate higher-twist contributions to inclusive meson photoproduction in the context of perturbative QCD, demonstrating that the higher-twist subprocess $\gamma q \to Mq$ contributes significantly to the inclusive cross section at large transverse momenta. The normalization of the subprocess is determined entirely by the meson electromagnetic form factor. We show that higher-twist effects are especially dramatic for ρ production.

I. INTRODUCTION AND FORMALISM

Among the fundamental predictions of QCD are asymptotic scaling laws for large-angle exclusive processes.[1,2] These reactions probe hadronic constituents at large relative momenta, or equivalently, the hadronic wave function at short distances. Important examples of exclusive amplitudes are provided by the electromagnetic form factors of mesons. These have been calculated within the framework of perturbative QCD.[3,4] Since there is little direct evidence with which to compare the predictions, it is fortunate that short-distance wave functions also control a wide variety of processes at large transverse momentum. In particular, the meson wave function determines the leading higher-twist contribution to meson photoproduction at high p_T.

Contributions to inclusive meson photoproduction $\gamma p \to MX$ fall into two categories: (1) minimum-twist reactions, such as $\gamma q \to gq$, followed by either quark or gluon fragmentation into the observed meson; and (2) higher-twist subprocesses, such as $\gamma q \to Mq$, in which the observed meson is made directly. The minimum-twist contributions depend on the quark and gluon fragmentation functions $D_q^M(z)$, $D_g^M(z)$. The higher-twist subprocesses are determined completely (to leading order) in terms of the meson electromagnetic form factor, $F_M(Q^2)$.

We will show that higher-twist terms contribute substantially to the inclusive meson cross section at moderate transverse momenta. In addition, we shall demonstrate that higher-twist reactions necessarily dominate in the kinematic limit where the transverse momentum approaches the phase-space boundary. In both domains, the trigger-bias effects[5] associated with quark fragmentation suppress the minimum-twist contributions. Thus we find that the reaction $\gamma p \to MX$ provides an important additional probe of the meson electromagnetic form factor. Inclusive meson photoproduction represents a significant test case in which higher-twist terms dominate those of minimum twist in certain kinematic domains.

We begin by reviewing the formalism for the meson form factor.[3] From Fig. 1 we see that the amplitude divides naturally into a short-distance Born amplitude folded together with two QCD-evolved wave functions. (Note that only the lowest $q\bar{q}$ Fock state contributes to the leading scaling behavior; other Fock-state contributions are suppressed by powers of $1/Q^2$.) The form factor may therefore be written

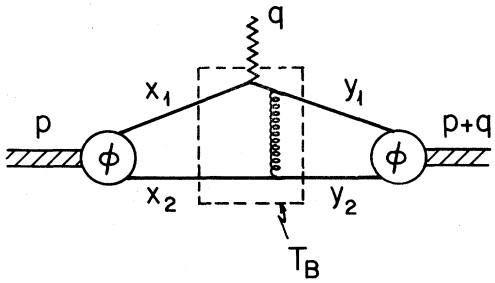

FIG. 1. A leading contribution to the meson form factor. Note that the amplitude divides into a short-distance Born amplitude and two QCD-evolved wave functions.

$$F_M(Q^2)=\int_0^1 \pi dx_i \pi dy_j \delta(1-x_1-x_2)\delta(1-y_1-y_2)\phi_M^\dagger(y_j,\bar{Q}^2)T_B(x_i,y_j,Q^2)\phi_M(x_i,\bar{Q}^2)\ , \tag{1}$$

where

$$T_B(x_i,y_j,Q^2)=\frac{16\pi C_F\alpha_S(\bar{Q}^2)}{Q^2}\left[\frac{e_1}{x_2y_2}+\frac{e_2}{x_1y_1}\right] \tag{2}$$

and

$$\phi_M(x_i,\bar{Q}^2)=x_1x_2\sum_{n=0}^{\infty}a_nC_n^{3/2}(x_1-x_2)\left[\ln\frac{\bar{Q}^2}{\Lambda^2}\right]^{-\gamma_n}\ . \tag{3}$$

$T_B(x_i,y_j,Q^2)$ represents the sum of all tree diagrams contributing to the hard-scattering subprocess $q_1\bar{q}_2\gamma\to q_1\bar{q}_2$, where e_1 is the charge of q_1 and e_2 the charge of $\bar{q}_2$. In Eq. (2) we have implicitly restricted M to a state of zero helicity. For mesons of nonzero helicity, angular momentum considerations suppress T_B by additional factors of m/Q. $\phi_M(x_i,\bar{Q}^2)$ is obtained from a ladderlike integral equation in the axial gauge; it is defined to contain all the $q\bar{q}$ two-particle-reducible bound-state graphs in the axial gauge. The $C_n^{3/2}$ are the Gegenbauer polynomials, while the γ_n are the standard anomalous dimensions. The coefficients a_n are determined by the boundary conditions on $\phi_M(x_i,\bar{Q}^2)$ at some $Q^2=Q_0^2$. Combining Eqs. (1), (2), and (3), we recover the QCD form factor for helicity-zero mesons,

$$F_M(Q^2)=\frac{4\pi C_F\alpha_s(\bar{Q}^2)}{Q^2}\left|\sum_{n=0,2,4\ldots}a_n\left[\ln\frac{\bar{Q}^2}{\Lambda^2}\right]^{-\gamma_n}\right|^2\ . \tag{4}$$

In Ref. 3, the scale-breaking terms in α_s and ϕ_M are evaluated at $\bar{Q}^2=Q^2$. Note, however, that $\bar{Q}^2$ is not determined in the leading-logarithmic approximation. It is only defined by higher-order corrections to T_B and ϕ_M. It has been suggested[6] that these corrections are minimized by using a momentum-subtracted two-loop version of α_s, evaluated at $\bar{Q}^2=|t_g|$, where t_g represents the momentum squared carried by the hard gluon in Fig. 1. On average,

$$Q^2=4|t_g|=4\bar{Q}^2 \tag{5}$$

for the form-factor calculation.

We shall adopt this approach. We set

$$\alpha_s(\bar{Q}^2)=4\pi\left[\frac{1}{\beta_0\ln\bar{Q}^2/\Lambda^2}-\frac{\beta_1}{\beta_0^3}\frac{\ln\ln\bar{Q}^2/\Lambda^2}{\ln^2\bar{Q}^2/\Lambda^2}\right]\ , \tag{6}$$

where Λ in (3) and (6) represents the QCD scale parameter in the momentum-subtraction (mom) scheme of Celmaster and Sivers.[7] In our calculation, we take $\Lambda=\Lambda_{\rm mom}=0.216$ GeV, corresponding to $\Lambda_{\overline{\rm MS}}=100$ MeV for $n_F=4$ (where $\overline{\rm MS}$ refers to the modified minimal-subtraction scheme). This value is representative of the results for the most recent deep-inelastic scattering experiments.[8] In addition, we allow for flavor thresholds in α_s as follows:

$$\begin{aligned} &n_F=3\ ,\ \Lambda=0.251\ \text{GeV}\ \text{ for }\bar{Q}\le 1.65\ \text{GeV}\ ,\\ &n_F=4\ ,\ \Lambda=0.216\ \text{GeV}\ \text{ for }1.65<\bar{Q}\le 4.73\ \text{GeV}\ ,\\ &n_F=5,\ \Lambda=0.165\ \text{GeV}\ \text{ for }\bar{Q}>4.73\ \text{GeV}\ . \end{aligned} \tag{7}$$

The Λ values for $n_F\neq 4$ are chosen to ensure continuity at the threshold boundaries. The one- and two-loop contributions to the β function

$$\beta_0=11-\tfrac{2}{3}n_F\ ,\beta_1=102-\tfrac{38}{3}n_F \tag{8}$$

depend on $\bar{Q}$ through n_F as specified in Eq. (7).

We shall treat the momentum dependence of ϕ_M in an analogous fashion. In Eq. (3), we take $\bar{Q}^2=|t_g|=Q^2/4$. Since higher-order corrections to the ϕ_M scale breaking have not been computed, we are forced to guess an appropriate value for Λ in Eq. (3). This and other fine points of our form-factor calculation are outlined in Appendix A.

Our computation for $F_\pi(Q^2)$ is shown in Fig. 2,

compared to available data.[9] We have assumed $\phi_\pi(x_i,\bar{Q}_0^2)\propto(x_1x_2)^{0.28}$ at $Q_0^2=2$ GeV^2. We have also normalized $\phi_\pi(x_i,\bar{Q}_0^2)$ against the weak decay amplitude $\pi\to\mu\nu$ which requires $a_0=\sqrt{3}f_\pi$. We shall use this determination of $F_\pi(Q^2)$ in Sec. II of this paper.

It is important to ask how sensitive the form-factor prediction is to our input conditions. The constraints of the low-Q^2 data and the asymptotic normalization a_0 do not entirely determine the form-factor prediction. For instance, we have compared our $\Lambda_{\overline{\rm MS}}=100$ MeV prediction with (a) the leading-logarithmic fit of Ref. 3, with $\phi(x_i,Q_0^2)\sim(x_1x_2)^{0.25}$ and $\Lambda^2=0.1$ GeV^2; and (b) a fit using our assumptions, with $\phi(x_i,\bar{Q}_0^2)\sim(x_1x_2)^{0.99}$ and Λ values corresponding to $\Lambda_{\overline{\rm MS}}=250$ MeV. The form factor in case (a) is indistinguishable from our $\Lambda_{\overline{\rm MS}}=100$ MeV prediction. The form factor for case (b) drops more rapidly at low Q^2 and is plotted in Fig. 2 along with the $\Lambda_{\overline{\rm MS}}=100$ MeV prediction. We will make a corresponding comparison for the higher-twist cross section.

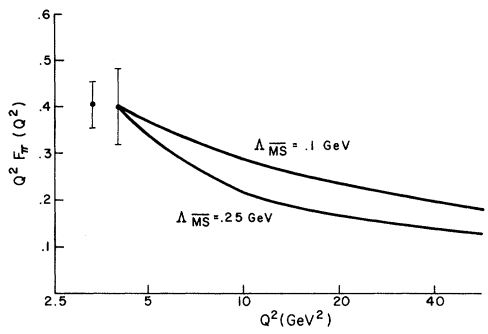

FIG. 2. The pion electromagnetic form factor, determined from Eq. (4). The data are from Ref. 6. The upper curve is for $\Lambda_{\overline{\rm MS}}=100$ MeV; the lower curve for $\Lambda_{\overline{\rm MS}}=250$ MeV.

For longitudinal ρ's, Eq. (4) still applies. The form for $F_{\rho_L}(Q^2)$ that we employ uses exactly the same initial condition for ϕ_{ρ_L} as for ϕ_π, changing only the overall normalization. We set $a_0=\sqrt{2}\sqrt{3}f_\rho$, where $f_\rho=0.107$ GeV is determined by the rate for $\rho\to e^+e^-$. There is, of course, no experimental form-factor data with which to verify that our assumptions for $\phi_{\rho_L}(x_i,\bar{Q}_0^2)$ are correct. Indeed, some of the first experimental measurements of F_{ρ_L} may occur through meson photoproduction.

We now turn to higher-twist reaction $\gamma q\to Mq$. The various diagrams contributing to this subprocess are shown in Fig. 3.[10] To leading order, we write the invariant amplitude in the form

$$\mathcal{M}_{\gamma q\to Mq}=\int\prod_i dx_i\,\delta(1-x_1-x_2)\,\phi_M(x,\text{“}Q^{2}\text{”})\,T_{\gamma q_1\to(q_1\bar{q}_2)q_2}\ , \tag{9}$$

where $T_{\gamma q_1\to(q_1\bar{q}_2)q_2}$ represents the sum of tree graphs contributing to $\gamma q_1\to(q_1\bar{q}_2)q_2$ with $q_1\bar{q}_2$ restricted to the spin state of M. The light-cone momentum fractions x_1 and $x_2=1-x_1$ specify the fractional momenta carried by q_1 and $\bar{q}_2$ in the Fock state. The determination of the "Q^2" scale will be discussed shortly. The $q_1\bar{q}_2$ spin state used in computing T may be written in the form

$$\chi^s_{q_1\bar{q}_2}=\sum_{s_1,s_2}\frac{u_{s_1}(x_1p_M)}{\sqrt{x_1}}\frac{\bar{v}_{s_2}(x_2p_M)}{\sqrt{x_2}}N^s_{s_1s_2}\ , \tag{10}$$

where the $N^s_{s_1s_2}$ project out a state of spin s. The factors $(\sqrt{x_1})^{-1}$ and $(\sqrt{x_2})^{-1}$ are purely conventional and fix the leading-order normalization of ϕ_M to be the same in Eqs. (1) and (5). In our calculation we neglected quark masses and used the following equivalent forms for $\chi^s_{q\bar{q}}$:

$$\chi^s_{q\bar{q}}=\begin{cases}\dfrac{\gamma_5\not{p}_M}{\sqrt{2}}, & \pi,\\[2ex] \dfrac{\not{p}_M}{\sqrt{2}}, & \rho_L \text{ helicity } 0\ ,\\[2ex] \mp\dfrac{\epsilon_\mp\not{p}_M}{\sqrt{2}}, & \rho_T \text{ helicity } \pm1\ ,\end{cases} \tag{11}$$

where $\epsilon_\pm=\mp(1/\sqrt{2})\,(0,1,\pm i,0)$ in a frame with $(p_M)_{1,2}=0$.

Evaluation of the x_i integral for any given tree graph is quite easy when $\phi_M(x_i,\text{“}Q^{2}\text{”})$ is symmetric under $x_1\leftrightarrow x_2$. This is a natural assumption for mesons composed of u and d quarks and is in fact a consequence of Eq. (3) for all mesons at large"Q^2". The x_i integral is always of the type

$$\int_0^1 dx\frac{\phi_M(x,\text{“}Q^{2}\text{”})}{x(1-x)}\begin{bmatrix}1\\ \text{or}\\ x\end{bmatrix}=\int_0^1 dx\frac{\phi_M(x,\text{“}Q^{2}\text{”})}{x(1-x)}\begin{bmatrix}1\\ \text{or}\\ \frac{1}{2}\end{bmatrix}\equiv I_M\,(\text{“}Q^{2}\text{”})\begin{bmatrix}1\\ \text{or}\\ \frac{1}{2}\end{bmatrix}\ , \tag{12}$$

where we have set $x_1=x$, $x_2=1-x$. From Eqs. (1) and (2) we see that the form factor contains the square of

$$\int_0^1 dx \frac{\phi_M(x,\bar{Q}^2)}{(1-x)} = \tfrac{1}{2} I_M(\bar{Q}^2) . \tag{13}$$

This allows us to completely determine the $\gamma q \to Mq$ cross section in terms of the meson form factor, through the relation

$$\frac{Q^2 F_M(Q^2)}{4\pi C_F \alpha_s(\bar{Q}^2)} = I_M{}^2(\bar{Q}^2) , \tag{14}$$

with $\bar{Q}^2 = Q^2/4$ as discussed earlier. Note that I_M is the only object in either calculation which cannot be determined entirely from first principles—it requires knowledge of the initial nonperturbative distribution amplitude $\phi_M(x_i,\bar{Q}_0{}^2)$. In principle, experimental measurement of F_M determines I_M and hence the $\gamma q \to Mq$ cross section.

We must now specify the values of "Q^2" at which α_s's and I_M's should be evaluated in the $\gamma q \to Mq$ subprocess calculation. As before, we adopt the position[8] that higher-order corrections to the connection through I_M between the form-factor and photoproduction calculations are minimized by (1) evaluating I_M ("Q^2") in Eq. (5) at

$$\text{"}Q^2\text{"} \mid = t_g \mid , \tag{15}$$

where t_g is the average squared momentum transfer carried by the hard gluon in a given subprocess; and (2) using the momentum-subtraction scheme for α_s and evaluating the α_s's in each subprocess at $\mid t_g \mid$.

For the s-channel graphs, Figs. 3(a) and 3(b), $t_g = \hat{s}/2$, while $t_g = \hat{u}/2$ for the u-channel contributions of Figs. 3(c) and 3(d). (Here $\hat{s}$, $\hat{t}$, and $\hat{u}$ are the standard Mandlestam invariants for the subprocess.) Higher-order calculations for both $F_M(Q^2)$ and $\gamma q \to Mq$ are required to ascertain if this procedure is successful. In particular, it should be noted that t_g is positive for s-channel graphs but negative for u-channel graphs and form-factor diagrams. Experience[11] with the Drell-Yan $\mu^+\mu^-$ production process suggests that higher-order corrections might be large for s-channel graphs. In order to have some estimate of the sensitivity of our calculation to the ansatz (15), we have checked that the very different choice of "Q^2" $= -\hat{t}$ in all $\gamma q \to Mq$ subprocess calculations has no visible effect on our final results.

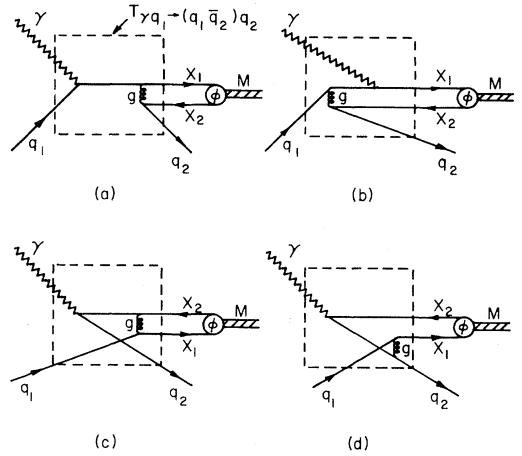

FIG. 3. The four leading contributions to the higher-twist subprocess $\gamma q \to Mq$. The hard-scattering amplitude $T_{\gamma q_1 \to (q_1 \bar{q}_2) q_2}$ is enclosed by a box. We characterize (a) and (b) as s-channel graphs and (c) and (d) as u-channel.

In light of the above discussion, we express the cross section for the higher-twist subprocess in terms of I_M:

$$\frac{d\sigma}{d\hat{t}}\bigg|_{\gamma q \to Mq}(\hat{s},\hat{t},\hat{u}) = \begin{cases} \dfrac{8\pi^2 \alpha C_F}{9}[\Delta(\hat{s},\hat{u}]^2 \dfrac{1}{\hat{s}^2(-\hat{t})}\left[\dfrac{1}{\hat{s}^2}+\dfrac{1}{\hat{u}^2}\right], & M=\pi,\rho_L \\ \dfrac{8\pi^2 \alpha C_F}{9}[\Delta(\hat{s},\hat{u})]^2 \dfrac{8(-\hat{t})}{\hat{s}^4 \hat{u}^2}, & M=\rho_T \end{cases} \tag{16}$$

where

$$\Delta(\hat{s},\hat{u}) = \left[\hat{u} e_1 \alpha_s \left[\frac{\hat{s}}{2}\right] I_M\left[\frac{\hat{s}}{2}\right] + \hat{s} e_2 \alpha_s \left[-\frac{\hat{u}}{2}\right] I_M\left[-\frac{\hat{u}}{2}\right]\right] , \tag{17}$$

$|t_g|$ sets the scale of I_M and α_s,[12] and I_M is related to the form factor through Eq. (14). The transverse ρ cross section has been summed over final helicities. It vanishes in the forward direction because of helicity-conservation conditions implicit in the tree graphs for $\gamma q \to (q\bar{q})q$.

Note that I_{ρ_T} is well defined even though $F_M(Q^2)$ differs from Eq. (4) for transverse mesons of nonzero helicity. Since I_{ρ_T} and $F_{\rho_T}(Q^2)$ are no longer linked through Eq. (14), photoproduction will be the most direct experimental handle on ϕ_{ρ_T}. In our calculation we set $\phi_{\rho_T}(x_i, \bar{Q}_0^2) = \phi_{\rho_L}(x_i, \bar{Q}_0^2)$, evolving ϕ_{ρ_T} to higher Q^2 with the anomalous dimensions appropriate for mesons of helicity one (see Appendix A).

Thus we see that the higher-twist cross section depends both on the momentum subtracted α_s and on the form factor $F_M(Q^2)$ through I_M. Roughly the relation takes the form $(d\sigma/d\hat{t})|_{\gamma q \to Mq} \propto \alpha_s F_M$. It is then interesting to ask how sensitive the higher-twist predictions are to the value of $\Lambda_{\overline{\rm MS}}$ employed. In Table I we give the $\alpha_s^{\rm mom}(Q^2)$ values for $\Lambda_{\overline{\rm MS}} = 100$ MeV and $\Lambda_{\overline{\rm MS}} = 250$ MeV. At low Q^2 it is clear that $\alpha_s^{\rm mom}$ is substantially larger for the higher $\Lambda_{\overline{\rm MS}}$ value. However, as demonstrated in Fig. 2, the form factor is generally somewhat smaller at low Q^2 for the higher $\Lambda_{\overline{\rm MS}}$. Thus we will discover that the predicted higher-twist cross section is only mildly influenced by the choice of $\Lambda_{\overline{\rm MS}}$. It should, of course, be kept in mind that this discussion of the sensitivity to $\Lambda_{\overline{\rm MS}}$ is in the context of our assumptions that the use of $\alpha_s^{\rm mom}$ ($|t_g|$) minimizes the higher-order corrections. We have also repeated the higher-twist calculations using a leading- logarithmic one-loop form for α_s with $\Lambda^2 = 0.1$ GeV^2, in conjunction with the leading-logarithmic $\Lambda^2 = 0.1$ GeV^2 fit to $F_\pi(Q^2)$ from Ref. 3. The results are very comparable to those for the $\Lambda_{\overline{\rm MS}} = 100$ MeV case.

The two subdiagrams contributing to the minimum-twist reaction $\gamma q \to gq$ are shown in Fig. 4. The corresponding cross section is easily verified:

$$\left.\frac{d\sigma}{d\hat{t}}\right|_{\gamma q \to gq}(\hat{s},\hat{t},\hat{u}) = -\frac{8\pi}{3} e_q^2 \alpha \frac{1}{\hat{s}^2}\left[\alpha_s(\hat{s})\frac{\hat{t}}{\hat{s}} + \alpha_s(-\hat{t})\frac{\hat{s}}{\hat{t}}\right] . \tag{18}$$

Following Ref. 6, the α_s's in Eq. (18) have been evaluated in the momentum-subtraction scheme, at momentum scales $|\hat{s}|$ and $|\hat{t}|$, representing the off-shell momenta carried by the hot quark propagators in Fig. 4. Other authors[13] have made other choices, such as $2\hat{s}\hat{t}\hat{u}/(\hat{s}^2+\hat{t}^2+\hat{u}^2)$, a form first employed by Feynman and Field.[14] Higher-order calculations are needed to determine the correct argument for α_s. Numerical results appear to be fairly insensitive to the choice of argument.

TABLE I. Values of the momentum-subtracted moving coupling constant.

Q^2 (GeV^2)	$\alpha_s(Q^2)$ $\Lambda_{\overline{\rm MS}} = 100$ MeV	$\alpha_s(Q^2)$ $\Lambda_{\overline{\rm MS}} = 250$ MeV
5	0.24	0.39
10	0.22	0.31
25	0.19	0.27
50	0.18	0.24
100	0.17	0.21

In general, many other subprocesses contribute to meson photoproduction, including (1) $\gamma q \to gq$ with $g \to M$, (2) $\gamma\bar{q} \to g\bar{q}$ with $g \to M$ or $\bar{q} \to M$, and (3) $\gamma\bar{q} \to M\bar{q}$. The subprocesses calculated earlier, however, dominate the minimum- and higher-twist cross sections. Indeed, they are the only contributions to the inclusive-cross-section difference,

$$\Delta_M = E\frac{d\sigma}{d^3p}(\gamma p \to M^+ X) - E\frac{d\sigma}{d^3p}(\gamma p \to M^- X) \equiv \Sigma_{M^+} - \Sigma_{M^-} . \tag{19}$$

The other subprocesses involving gluons or antiquarks contribute equally to Σ_{M^+} and Σ_{M^-} and cancel in the charge difference.

In our calculation, we ignore hadronized photons. Hadronized photons make major contributions to Σ_{M^+} and Σ_{M^-} at low to moderate p_T.

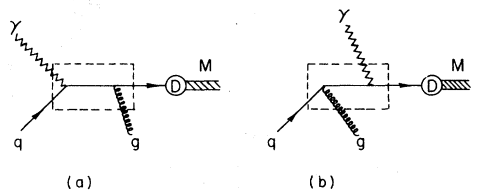

FIG. 4. The two leading contributions to the minimum-twist subprocess $\gamma q \to gq$, $q \to M$. The hard-scattering amplitude is enclosed by a box. $D_{M/q}$ represents the quark fragmentation function into a meson M.

These contributions tend to cancel in the charge-difference cross section Δ_M.[13] They cancel completely for photoproduction off isoscalar targets.

We now incorporate the higher-twist (HT) subprocess $\gamma q \to Mq$ into the full inclusive cross section. From Fig. 5 we see that the photon and the meson may be viewed as an effective current striking the incoming quark line. With this in mind, we write the complete cross section in formal analogy with deep-inelastic scattering,[15]

$$\Sigma_M^{\rm HT} \equiv E\frac{d\sigma^{\rm HT}}{d^3p}(\gamma p \to MX) = \frac{1}{\pi}\int_0^1 dx\, \delta(\hat{s}+\hat{t}+\hat{u})\hat{s}G_{q/p}(x,-\hat{t})\frac{d\hat{\sigma}}{d\hat{t}}\Big|_{\gamma q\to Mq}(\hat{s},\hat{t},\hat{u}), \tag{20}$$

where the subprocess invariants

$$\hat{s}=xs,\quad \hat{t}=t,\quad \hat{u}=xu \tag{21}$$

are given in terms of the invariants of the overall reaction

$$s=(p_p+p_\gamma)^2,\quad t=(p_\gamma-p_M)^2=-\frac{s}{2}(x_R-x_F),\quad u=(p_p-p_M)^2=-\frac{s}{2}(x_R+x_F) \tag{22}$$

with $x_R=(x_F^2+x_T^2)^{1/2}$. Here $x_F=2(p_M)_{||}/\sqrt{s}$ and $x_T=2(p_M)_\perp/\sqrt{s}\equiv 2p_T/\sqrt{s}$ specify the longitudinal and transverse momentum of the meson. In terms of these the rapidity of M is given by

$$y=\tfrac{1}{2}\ln[(x_R+x_F)/(x_R-x_F)].$$

For the minimum-twist (MT) contribution, we find[15]

$$\Sigma_M^{\rm MT}=E\frac{d\sigma^{\rm MT}}{d^3p}(\gamma p\to MX)=\frac{1}{\pi}\int_0^1 dx\int_0^1\frac{dz}{z^2}\delta(\hat{s}+\hat{t}+\hat{u})\hat{s}G_{q/p}(x,-\hat{t})D_{M/q}(z,-\hat{t})\frac{d\hat{\sigma}}{d\hat{t}}\Big|_{\gamma q\to gq}(\hat{s},\hat{t},\hat{u}), \tag{23}$$

where

$$\hat{s}=xs,\quad \hat{t}=\frac{t}{z},\quad \hat{u}=\frac{xu}{z}. \tag{24}$$

$D_{M/q}(z,-\hat{t})$ represents the quark fragmentation function into a meson containing a quark of the same flavor.

For pions the fragmentation function has been chosen in two ways: (a) from the data for $\nu p\to\mu^-\pi^+X$, which measures $D_{\pi^+/u}(z,-\hat{t})$ directly;[16] and (b) from the Feynman-Field analytic form for $D_{\pi^+/u}(z,-\hat{t})$, which represents a good global fit to a variety of data.[17] The two choices are compared in Fig. 6. We found little difference in the results for (a) and (b) and will use (b) in Sec. II of this paper. For ρ's, of course, direct data is not available. We shall use the Feynman-Field forms for $D_{\rho/q}(z,-\hat{t})$, also illustrated in Fig. 6.

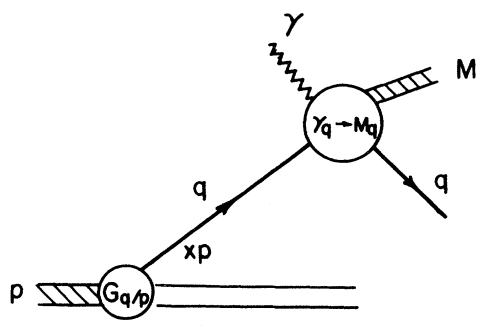

FIG. 5. The embedding of the higher-twist subprocess $\gamma q\to Mq$ into the inclusive cross section. Note that the photon and the meson may be viewed as an effective current striking the quark line, in analogy with deep-inelastic scattering.

In our numerical work we use the Buras-Gaemers parametrization for the quark distribution functions $G_{q/p}(x,-\hat{t})$.[18] These have been extracted directly from deep-inelastic data for $W_2(x,Q^2)$. From Fig. 5 we see that regarding the photon and the meson as an effective current fixes $Q^2=-\hat{t}$, where $\hat{t}$ is precisely the squared momentum transfer absorbed by the quark. This choice should minimize higher-order corrections.[6,7]

Finally we note that although we evaluate our minimum-twist subprocess $\gamma q\to gq$ with external lines on shell, we do not allow for transverse-momentum fluctuations of the initial quark. It has been demonstrated[19] that such a procedure is incorrect, and that one should simply expand the cross section in terms of minimum- and higher-twist subprocesses convoluted with QCD-evolved distribution functions. Inclusive meson photopro-

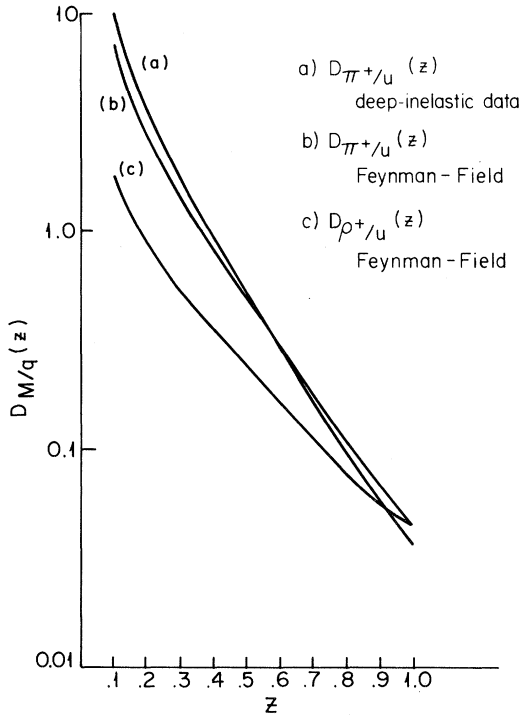

FIG. 6. The quark fragmentation functions (a) $D_{\pi^+/u}(z)$, from deep-inelastic neutrino data; (b) $D_{\pi^+/u}(z)$, from the Feynman-Field analytic form; and (c) $D_{\rho^+/u}(z)$, from Feynman and Field.

duction is one of the simplest cases for which this expansion, including the relative normalization of the various contributions, can be computed systematically within the framework of perturbative QCD.

II. RESULTS AND DISCUSSION

We now turn to our results. We have computed the M^+ and M^- inclusive cross sections Σ_{M+} and Σ_{M-} as well as the charge-difference cross section $\Delta_M = \Sigma_{M+} - \Sigma_{M-}$, considering only the dominant contributions to inclusive meson photoproduction:

$$\gamma q \to gq \searrow_M$$

labeled MT for minimum twist, and

$$\gamma q \to Mq$$

labeled HT for higher twist. Our calculations were performed for $M=\pi$, ρ_L, and ρ_T at $\sqrt{s}=7$, 14.1, and 25 GeV.

We illustrate the general features of our results with an example which can be compared directly to the minimum-twist results of Fontannez *et al.* for π production at $\sqrt{s}=14.1$ GeV.[13] A plot of Δ_π and Σ_{π^-} vs p_T at $y=0.5$ appears in Fig. 7(a) and of Δ_π and Σ_{π^-} vs y at $p_T=3.0$ GeV/c in Fig. 7(b). These plots are for the Λ values of Eq. (7) corresponding to $\Lambda_{\overline{\rm MS}}=100$ MeV. The minimum-twist results for Δ_π and Σ_{π^-} are slightly smaller than those of Fontannez *et al.* because of the smaller value of $\Lambda_{\overline{\rm MS}}$ we have employed. To indicate the sensitivity to $\Lambda_{\overline{\rm MS}}$ of both minimum- and higher-twist terms, we present in Fig. 7(c) the results for Δ_π and Σ_{π^-} as a function of p_T, computed using the α_s values and form-factor fit corresponding to $\Lambda_{\overline{\rm MS}}=250$ MeV. In Figs. 8 and 9 we plot the ratios of higher twist to minimum twist for Σ_{π^+}, Σ_{π^-} and Δ_π computed in the $\Lambda_{\overline{\rm MS}}=100$ MeV case.

These figures reveal the following general features. In the $\Lambda_{\overline{\rm MS}}=100$ MeV case, the higher-twist contribution to Σ_{π^-} is generally comparable to the minimum-twist contribution at all transverse momenta. The effect of higher-twist diagrams on Δ_π is smaller because $\Sigma^{HT}_{\pi^+} \approx \Sigma^{HT}_{\pi^-}$ at moderate p_T (near 4 GeV/c in this case). Nevertheless, $|\Delta^{HT}_\pi/\Delta^{MT}_\pi| > 1$ at the highest p_T values. In the $\Lambda_{\overline{\rm MS}}=250$ MeV case, the higher-twist contributions are somewhat larger. The minimum-twist predictions are also somewhat larger with the result that the relative contributions of minimum- and higher-twist processes are fairly independent of $\Lambda_{\overline{\rm MS}}$.

The general features of these graphs are easily understood:

(a) $\Sigma^{\rm HT}_{\pi^+} = \Sigma^{\rm HT}_{\pi^-}$ at some p_T since $\Sigma^{\rm HT}_{\pi^+} \propto G_{u/p} e_d{}^2$ while $\Sigma^{\rm HT}_{\pi^-} \propto G_{d/p} e_u{}^2$, where this leading behavior is extracted from the dominant u-channel contributions to the higher-twist subprocess. The change in quark charge tends to compensate the change in distribution function, leading to higher-twist cross sections $\Sigma^{\rm HT}_{\pi^+}$ and $\Sigma^{\rm HT}_{\pi^-}$ of approximately the same order.

(b) $\Sigma^{\rm MT}_{\pi^+} > \Sigma^{\rm MT}_{\pi^-}$ at all p_T since $\Sigma^{\rm MT}_{\pi^+} \propto G_{u/p} e_u{}^2$ while $\Sigma^{\rm MT}_{\pi^-} \propto G_{d/p}\, e_d{}^2$. The smaller quark charge e_d and the smaller distribution function $G_{d/p}$ both work to suppress $\Sigma^{\rm MT}_{\pi^-}$. Thus, combining with (a), it is not surprising that $\Sigma^{\rm HT}_{\pi^-} \approx \Sigma^{\rm MT}_{\pi^-}$ in most kinematic domains, while $\Sigma^{\rm MT}_{\pi^+}$ is generally larger than $\Sigma^{\rm HT}_{\pi^+}$.

(c) Higher twist tends to dominate minimum twist near the phase-space boundary. Naive power

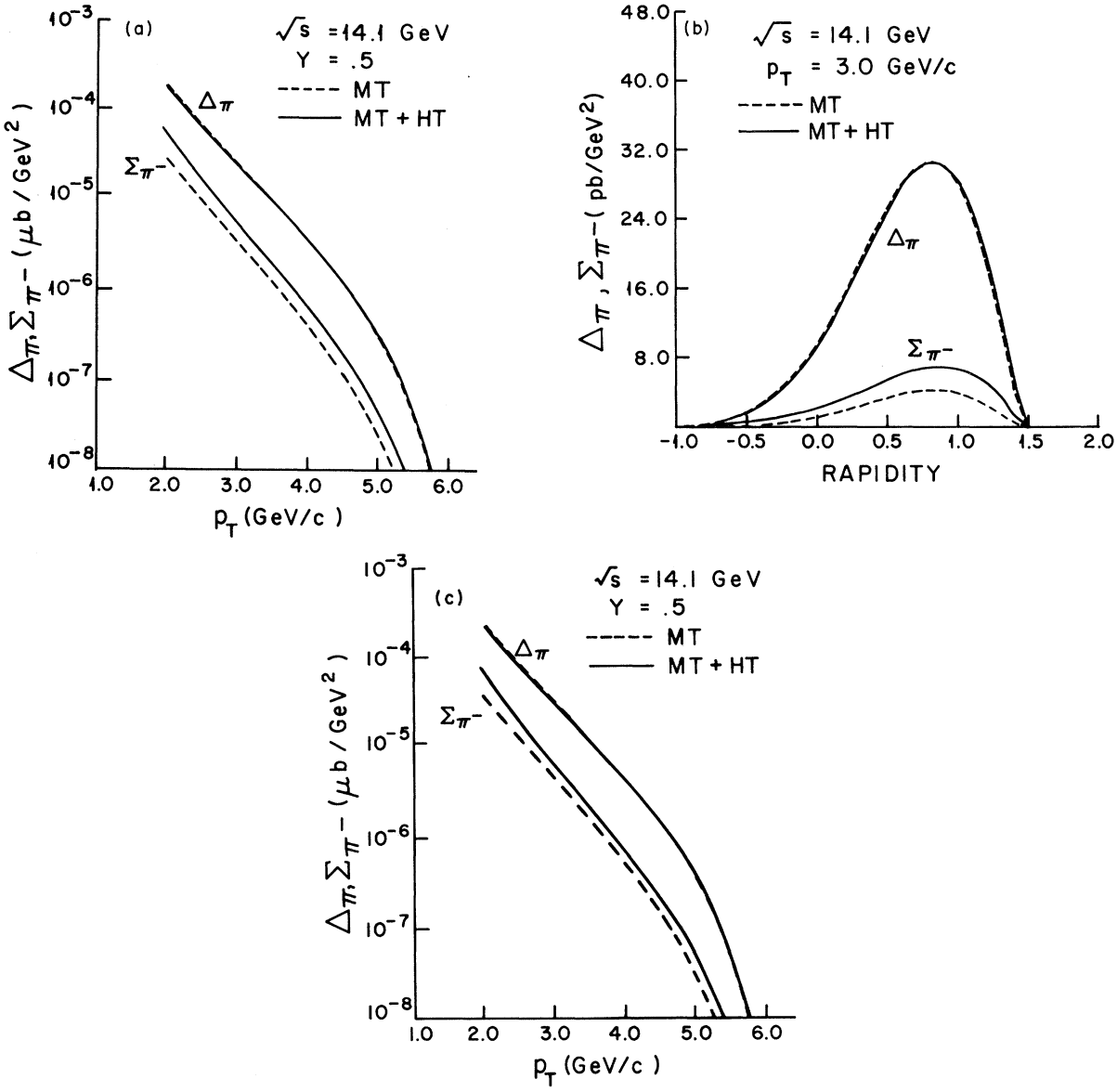

FIG. 7. Minimum- and higher-twist contributions to inclusive π production at $\sqrt{s}=14.1$ GeV. $\Lambda_{\overline{\rm MS}}=100$ MeV for (a) and (b); $\Lambda_{\overline{\rm MS}}=250$ MeV for (c).

counting gives

$$\Sigma^{\rm HT}90^\circ \underset{\sim}{\alpha_s}\frac{(1-x_T)^3}{{p_T}^6} \tag{25}$$

versus

$$\Sigma^{\rm MT}90^\circ \underset{\sim}{\alpha_s}\frac{(1-x_T)^5}{{p_T}^4}\ .$$

The necessity of making M indirectly in the minimum-twist case suppresses the MT mechanism as $x_T\to 1$, despite the lower associated p_T power damping.

(d) The difference in powers of α_s and p_T mentioned above means that higher-twist reactions are more rapidly enhanced as p_T decreases. Thus higher-twist processes can become dominant at lower transverse momenta. We do not present results below $p_T=2$ GeV/c, however, because perturbation theory becomes increasingly less reliable in that domain.

(e) $\Sigma^{\rm HT}_{\pi^+}>\Sigma^{\rm HT}_{\pi^-}$ at high p_T whereas the reverse is

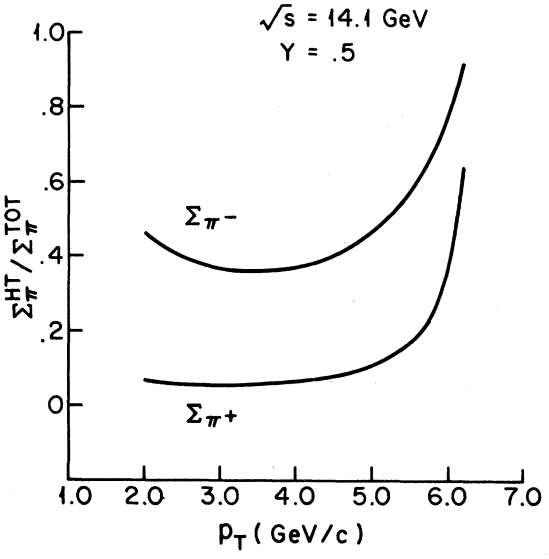

FIG. 8. $\Sigma_\pi^{HT}/\Sigma_\pi^{TOT}$ at $\sqrt{s}=14.1$ GeV, $\Lambda_{\overline{MS}}=100$ MeV.

true at low p_T because $G_{d/p}(x)/G_{u/p}(x)\sim(1-x)$ —higher transverse momenta probe higher values of x [see Eq. (20)], suppressing the d quark necessary for π^- production. At lower transverse momenta $G_{d/p}$ becomes comparable to $G_{u/p}$, favoring

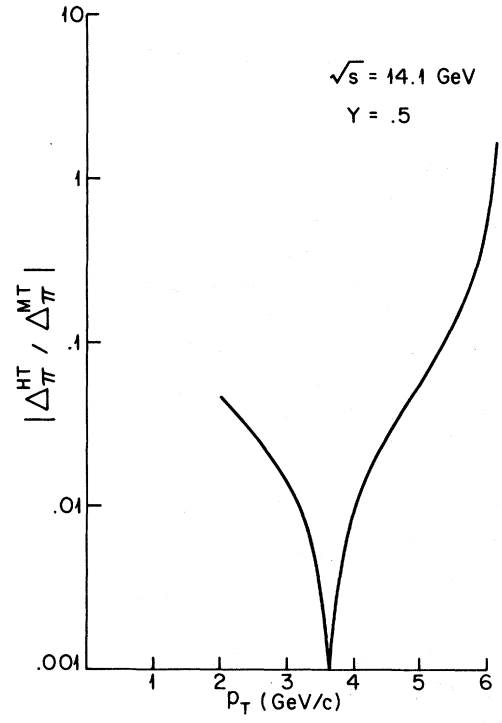

FIG. 9. $|\Delta_\pi^{HT}/\Delta_\pi^{MT}|$ at $\sqrt{s}=14.1$ GeV, $\Lambda_{\overline{MS}}=100$ MeV.

π^- production because of the quark charge argument outlined in (a) above. Thus Δ_π^{HT} becomes negative for lower p_T (in the range of 2 GeV/c to 3 GeV/c). For larger values of $\sqrt{s}$ the region over which $\Delta_\pi^{HT}<0$ extends to larger p_T since x decreases with $\sqrt{s}$.

The rapidity dependence of Σ_{π^-} and Δ_π, shown in Fig. 7(b), illustrates the tendency of the higher-twist terms to be enhanced in the domain of negative rapidity. In this region $\hat{u}$ must be small because the overall subprocess center of mass always moves with positive rapidity. Only the higher-twist subprocesses have the $1/\hat{u}$ structure necessary to enhance this region. The minimum-twist subprocesses have $1/\hat{t}$ terms which prefer the forward direction.

Plots similar to those presented at $\sqrt{s}=14.1$ GeV are given for $\sqrt{s}=7$ GeV and $\sqrt{s}=25$ GeV in Figs. 10 and 11 respectively, for $\Lambda_{\overline{MS}}=100$ MeV. In these cases we have chosen to plot the p_T distributions at $y=0$ and the rapidity distributions at $p_T=3$ GeV/c. These choices are fairly representative, with higher-twist contributions to Δ_π on the same order as those of minimum twist. As expected from Eq. (25), we see from Fig. 10(a) that the relative higher-twist contribution to Σ_{π^-} is largest for lower $\sqrt{s}$ values at fixed p_T. Nevertheless, even at $\sqrt{s}=25$ GeV, Fig. 11(a) shows that higher-twist contributions are important to Δ_π below $p_T=3.5$ GeV/c. Although not shown, they are also important above $p_T=12$ GeV/c, near the phase-space boundary. At $\sqrt{s}=25$ GeV, HT contributions are important to Σ_{π^-} at all values of p_T.

The preceding results demonstrate that higher-twist contributions must indeed be considered in regions of low to moderate p_T as well as near the phase-space boundaries at all energies in π production. Higher-twist contributions are even more important in ρ production. It becomes difficult to find a region of $\sqrt{s}$ and p_T in which higher-twist terms are suppressed. In fact, over much of the moderate $\sqrt{s}$ region we have studied, higher-twist terms dominate those of minimum twist. The reasons behind the relative enhancement of higher twist in the case of the ρ are quite simple:

(i) The minimum-twist contributions to ρ production are generally comparable to or slightly lower than those for π production. This follows simply from the fact that the rho fragmentation functions $D_{\rho^+/u}$ and $D_{\rho^-/d}$ are generally smaller than the pion fragmentation functions $D_{\pi^+/u}$ and $D_{\pi^-/d}$, as shown in Fig. 6.

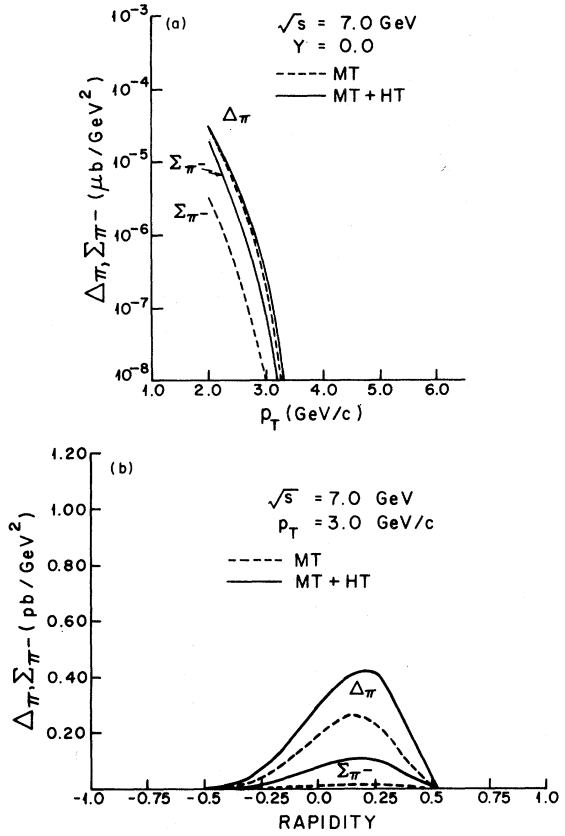

FIG. 10. π production at $\sqrt{s}=7$ GeV, $\Lambda_{\overline{\rm MS}}=100$ MeV.

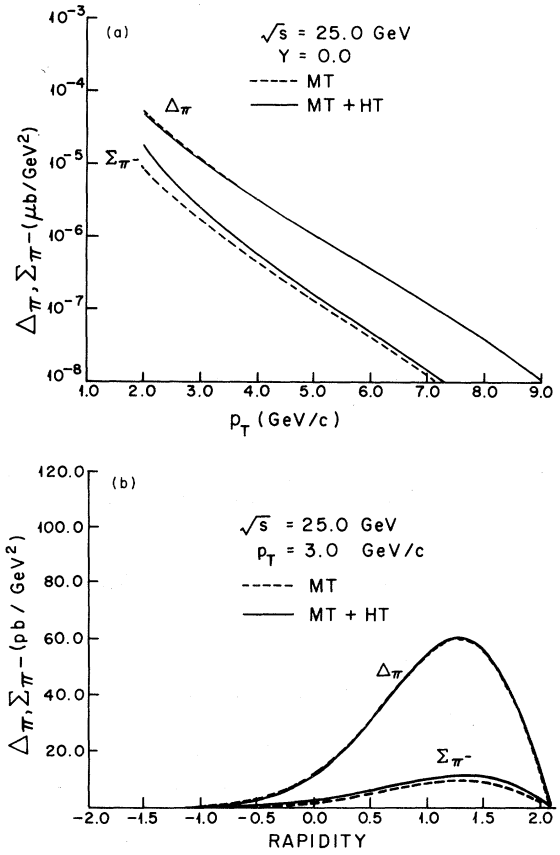

FIG. 11. π production at $\sqrt{s}=25$ GeV, $\Lambda_{\overline{\rm MS}}=100$ MeV.

(ii) In contrast, the contributions from higher-twist terms are generally larger. The longitudinal ρ_L cross section is normalized to be a factor of $2f_\rho^2/f_\pi^2\approx 2.5$ times larger than the corresponding π cross section. The transverse ρ_T cross sections are generally at least as large. Of course, all three polarizations contribute, further enhancing the higher-twist cross section.

Thus we have the situation illustrated in Figs. 12 and 13, computed for $\Lambda_{\overline{\rm MS}}=100$ MeV. At $y=0.5$ and $\sqrt{s}=14.1$ GeV, Fig. 12(a), higher-twist terms dominate even the $\Sigma_{\rho+}$ cross sections at all values of p_T. The rapidity dependence at $p_T=3$ GeV/c and $\sqrt{s}=14.1$ GeV, Fig. 12(b), demonstrates that this is generally true for all y. We find substantial contributions from higher-twist terms at $\sqrt{s}=25$ GeV, $y=0$. Figure 13(a) shows that only in Δ_ρ where the higher-twist terms tend to cancel above $p_T=6$ GeV/c can one find a domain where minimum twist dominates. In the two separate cross sections, $\Sigma_{\rho+}$ and especially $\Sigma_{\rho-}$, higher-twist terms are very significant at all p_T. Note that $\Delta_\rho^{\rm TOTAL}<0$ for $p_T\lesssim 3$ GeV/c, well into the perturbative domain ($p_T\gtrsim 2$ GeV/c). This signature alone would provide dramatic confirmation of the presence of higher-twist contributions. Figure 13(b) shows the rapidity dependence at $\sqrt{s}=25$ GeV, $p_T=3$ GeV/c. Again, the dominance of higher-twist terms is apparent at this value of p_T and all values of y. For $\Lambda_{\overline{\rm MS}}=250$ MeV, the higher-twist terms are even more important.

In conclusion, we have seen that the reactions $\gamma p\to\pi X$ and $\gamma p\to\rho X$ receive very significant contributions from the higher-twist subprocess $\gamma q\to Mq$. These probe the meson form factors over a large range of "Q^2" [$-\hat{u}/2$ and $+\hat{s}/2$ in (16) and (17)]. For $p_T=2$ GeV/c, $\hat{s}/2$ never falls below 10 GeV^2, while $-\hat{u}/2$ is always greater than 2 GeV^2.[20] At larger values of p_T, $\hat{s}/2$ ranges as high as 300 GeV^2 and $-\hat{u}/2$ as high as 150 GeV^2. In Table II we present sample values of "Q^2" for $p_T=2$ GeV/c and for p_T near the phase-space boundary. From this table we see that the kinematic domains in which the higher-twist con-

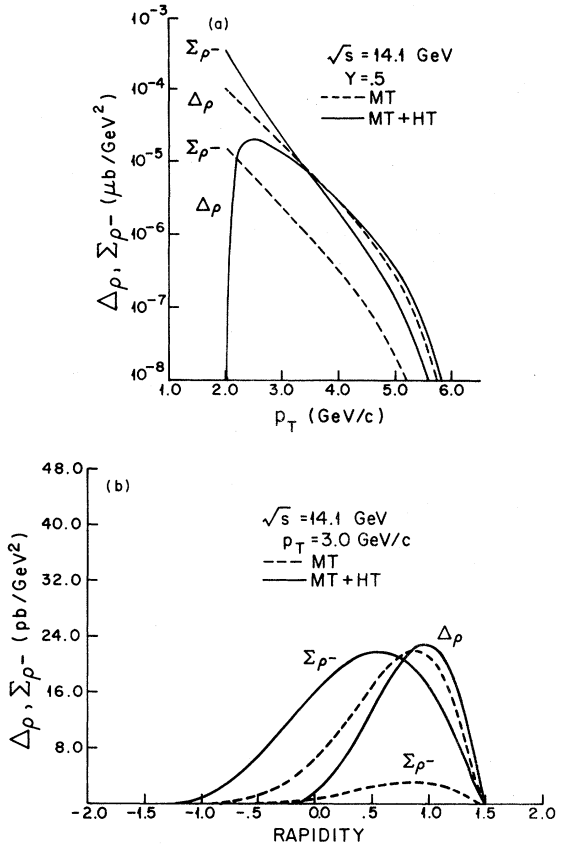

FIG. 12. ρ production at $\sqrt{s}=14.1$ GeV, $\Lambda_{\overline{\rm MS}}=100$ MeV.

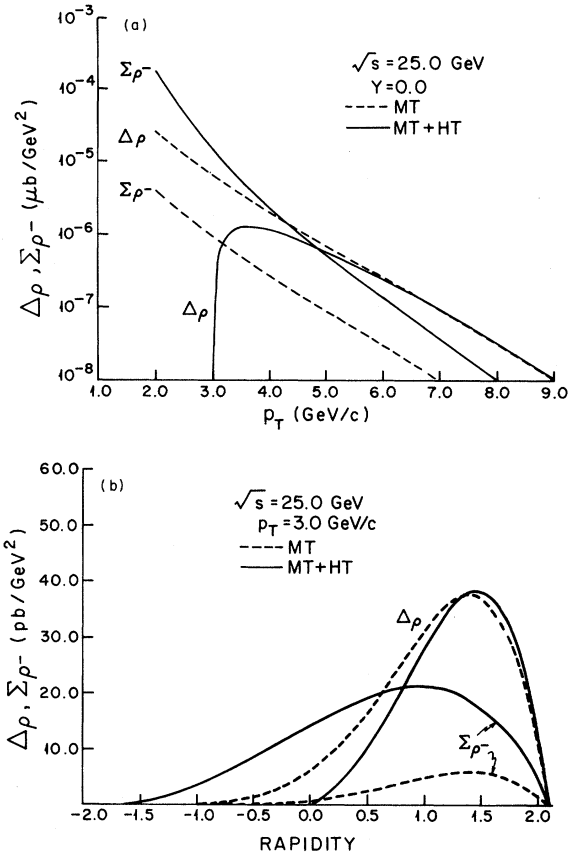

FIG. 13. ρ production at $\sqrt{s}=25$ GeV, $\Lambda_{\overline{\rm MS}}=100$ MeV.

tributions dominate meson production provide a truly unique and direct probe of the form factor of the meson. The cross sections for negative meson production, Σ_{π^-} and Σ_{ρ^-}, are especially sensitive to the higher-twist subprocess. A careful study of the meson photoproduction reactions over the full range of Fermilab $\sqrt{s}$ values and at high p_T is highly desirable, both as an important probe of the meson form factor and as a significant test of higher twist in QCD.

TABLE II. Sample "Q^2" values probed by higher twist.

$\sqrt{s}$ (GeV)	y	p_T (GeV/c)	$-\hat{u}/2$ (GeV^2)	$\hat{s}/2$ (GeV^2)
7.0	0	2.0	2.8	9.8
7.0	0	3.4	11.2	23.1
14.1	0.5	2.0	2.6	11.2
14.1	0.5	6.17	67.8	94.3
25.0	0	2.0	2.2	27.2
25.0	0	6.0	23.7	98.6
25.0	0	12.4	152.5	307.5

ACKNOWLEDGMENTS

We would like to thank S. J. Brodsky for helpful conversations. J. A. B. holds a National Science Foundation Graduate Fellowship. J. F. G. is supported by the A. P. Sloan Foundation and by the Department of Energy under Contract No. DE-AS03-76SF00034PA191. J. F. G. would like to thank the Institute for Theoretical Physics at Santa Barbara where the manuscript was written. We would like to thank the Stanford Linear Accelerator Center for its hospitality during the initial stages of this work.

APPENDIX A

In this appendix we provide more details about our determination of the π and ρ_L form factors.

We first specify the anomalous dimensions γ_n used in Eqs. (3) and (4),

$$\gamma_n=\frac{C_F}{\beta_0}\left[1+4\sum_{k=2}^{n+1}\frac{1}{k}-\frac{2\delta_{h_1\bar{h}_2}}{(n+1)(n+2)}\right], \tag{A1}$$

where $\delta_{h_1\bar{h}_2}=1$ for π's and longitudinally polarized ρ_L's and $\delta_{h_1\bar{h}_2}=0$ for transverse ρ_T's. We use the one-loop beta function in γ_n,

$$\beta_0=11-\tfrac{2}{3}n_F\ , \tag{A2}$$

with n_F depending on Q through the flavor thresholds:

$$n_F=\begin{cases}3, & Q\le 1.65\ \text{GeV},\\ 4, & 1.65<Q\le 4.73\ \text{GeV},\\ 5, & Q>4.73\ \text{GeV}.\end{cases} \tag{A3}$$

The two-loop expression for α_s is used in the form-factor calculations, as specified in the text. We have chosen Λ in Eq. (3) to be equal to $\Lambda_{\overline{\rm MS}}$.

We have compared the pion form-factor predictions for two values of $\Lambda_{\overline{\rm MS}}$, 100 and 250 MeV. The form factor in each case was constrained to agree with the low-Q^2 pion data, and we imposed the correct normalization on a_0 in both cases. The starting forms of ϕ were

$$\phi_M(x_i,\bar{Q}_0^2)=N_M\times\begin{cases}(x_1x_2)^{0.28}\ , & \Lambda_{\overline{\rm MS}}=100\ \text{MeV}\ ,\\ (x_1x_2)^{0.99}, & \Lambda_{\overline{\rm MS}}=250\ \text{MeV}\end{cases} \tag{A4}$$

at $\bar{Q}_0^2=Q_0^2/4$ with $Q_0^2=2\ \text{GeV}^2$.

The constant N_M is chosen so that

$$a_0=3\int_{-1}^{1}d(x_1-x_2)C_0^{3/2}(x_1-x_2)\phi_M(x_i,\bar{Q}_0^2) \tag{A5}$$

yields

$$a_0=\sqrt{3}f_\pi\quad(f_\pi=93\ \text{MeV}) \tag{A6}$$

for the pion fits. When making predictions for the ρ form factor we used the same starting ϕ_M forms, renormalized by requiring

$$a_0=\sqrt{6}f_\rho\quad(f_\rho=107\ \text{MeV}) \tag{A7}$$

for both longitudinal and transverse ρ's. The two pion fits are compared in Fig. 2. These fits include a subasymptotic multiplication factor of $(1+m_\rho^2/Q^2)^{-1}$. In addition, we reiterate that the $\Lambda^2=0.1\ \text{GeV}^2$ leading order fit of Ref. 3 is indistinguishable from our $\Lambda_{\overline{\rm MS}}=100$ MeV fit.

---

[1]Early work appears in S. J. Brodsky, R. Blankenbecler, and J. F. Gunion, Phys. Lett. 39B, 649 (1972); Phys. Rev. D 6, 2651 (1972).

[2]QCD counting rules were formalized by S. J. Brodsky and G. R. Farrar, Phys. Rev. Lett. 31, 1153 (1973) and V. A. Matveev, R. M. Muradyn, and A. V. Tavkhelidze, Lett. Nuovo Cimento 1, 719 (1973).

[3]G. P. Lepage and S. J. Brodsky, Phys. Lett. 87B, 359 (1979); Phys. Rev. Lett. 43, 545 (1979); 43, 1625 (E) (1979); Phys. Rev. D 22, 2157 (1980).

[4]A. Duncan and A. H. Mueller, Phys. Lett. 90B, 159 (1980); Phys. Rev. D 21, 1636 (1980).

[5]S. D. Ellis, P. V. Landshoff, and M. Jacob, Nucl. Phys. B108, 93 (1978); P. V. Landshoff and M. Jacob, Nucl. Phys. B113, 395 (1976).

[6]W. Celmaster and D. Sivers, [Report No. ANL-HEP-PR-80-61, 1980 (unpublished)] first developed an analogous conclusion in high-p_T physics. R. Field, R. Gupta, S. Otto, and L. Chang [Nucl. Phys. B186, 429 (1981)] have examined this question for $F_\pi(Q^2)$ and concluded that $\alpha_s(t_g/4)$ might be better in this case.

[7]W. Celmaster and D. Sivers, Phys. Rev. D 23, 227 (1981).

[8]See *Proceedings of the 1981 International Symposium on Lepton and Photon Interactions at High Energies, Bonn,* edited by W. Pfeil (Universität Bonn, Bonn, 1981).

[9]C. Bebeck *et al.*, Phys. Rev. D 13, 25 (1976).

[10]Subprocesses of interest are surveyed in R. Blankenbecler, S. J. Brodsky, and J. F. Gunion, Phys. Rev. D 18, 900 (1978).

[11]For a review see F. Vanucci, Moriond Conference, Les Arcs, France, 1981 (unpublished).

[12]Note that the e_1 and e_2 terms arise from two separate sets of graphs—each set is gauge invariant. Thus the differing α_s and I_M arguments do not destroy gauge invariance.

[13]M. Fontannaz, A. Mantrach, B. Pire, and D. Schiff, Phys. Lett. 89B, 263 (1980).

[14]See R. D. Field, R. P. Feynman, and G. C. Fox, Phys. Rev. D 18, 3320 (1978); R. D. Field, in *Proceedings of the 19th International Conference on High Energy Physics, Tokyo, 1978,* edited by S. Homma, M. Kawaguchi, and H. Miyazawa (Phys. Soc. of Japan, Tokyo, 1979).

[15]See Ref. 7 and D. Jones and J. F. Gunion, Phys. Rev. D 19, 867 (1979).

[16]N. Schmitz, in *Proceedings of the 1979 International Symposium on Lepton and Photon Interactions at High Energies Fermilab,* edited by T. B. W. Kirk and H. D. I. Abaranel (Fermilab, Batavia, Illinois, 1980). See also P. Allen *et al.*, Phys. Lett. 96B, 209 (1980) and Nucl. Phys. B176, 269 (1980). See also N. Schmitz, Acta Phys. Pol. B11, 913 (1980).

[17]R. Feynman and R. Field, Nucl. Phys. B136, 1 (1978).

[18]A. J. Buras and K. J. F. Gaemers, Nucl. Phys. B132, 249 (1978).

[19]S. J. Brodsky, R. R. Horgan, W. E. Caswell, Phys. Rev. D 18, 2415 (1978); H. D. Politzer, Nucl. Phys. B172, 349 (1980).

[20]From Eqs. (20)–(22) we find that at $y=0$ ($x_F=0$)

$$\frac{-\hat{u}}{2}=\frac{p_T{}^2/2}{1-p_T\sqrt{s}}\ ,\quad \frac{\hat{s}}{2}=\frac{p_T{}^2\sqrt{s}\,/2}{1-p_T/\sqrt{s}}\ .$$